Polarization Modulation at Last Quantum Barrier for High Efficiency AlGaN-Based UV LED

Zhiyuan Liu, Yi Lu, Yue Wang, Rongyu Lin, Chenxin Xiong, and Xiaohang Li, *Member, IEEE*

***Abstract*—The performance of AlGaN-based light-emitting diodes (LEDs) emitting at UVA–UVC regions can be severely compromised due to the polarization difference (ΔP) between the last quantum barrier (LQB) and the electron blocking layer (EBL). In this work, the different situations of the bandgap difference (ΔE_g) and ΔP of InAlN/AlGaN and AlGaN/AlGaN heterojunctions fully strained on GaN and AlN substrates are discussed. It shows that the InAlN/AlGaN heterojunctions could produce positive or negative sheet charges at the heterointerface under $\Delta E_g > 0$, which could not be realized by the conventional AlGaN/AlGaN heterojunctions. To demonstrate and utilize the feature, the polarization-modulated InAlN LQBs with 0.14–0.16 indium compositions of 320 nm UVB LEDs are designed and investigated. It is observed that the InAlN LQBs could replace the conventional AlGaN LQB to improve electron confinement and hole injection by affecting effective barrier heights. By modulating the LQB/EBL polarization using InAlN, the proposed UV LED has a 32% enhancement in internal quantum efficiency and lower efficiency droop (from 16.9% to 0.7%) compared with the conventional one without modulation. The operation voltage at the same current also significantly decreases. The improvement of optical output power and wall plug efficiency at 60 mA in proposed structures are near 90% and 100%, respectively. This study provides a novel and highly effective methodology for development of high efficiency UV LEDs.**

***Index Terms*—AlGaN-based UV LED, electron blocking, hole injection, indium aluminum nitride, last quantum barrier, polarization.**

I. Introduction

RECENTLY, AlGaN-based UV light-emitting diodes (LEDs) have undergone accelerating development due to important applications such as UV curing, phototherapy, sensing, and disinfection. Compared with conventional UV sources such as mercury lamps, UV LEDs are reliable, compact, and ecofriendly [1]. However, UV LEDs still suffer from low internal quantum efficiency (IQE) due to Auger recombination, Shockley–Read–Hall (SRH) recombination, electron overflow, and constrained hole injection, etc. [2]–[7].

Manuscript received November 1, 2021; revised December 14, 2021; accepted December 24, 2021. Date of publication December 29, 2021; date of current version January 19, 2022. This work was supported in part by the KAUST Baseline Fund under Grant BAS/1/1664-01-01, and in part by the KAUST Competitive Research under Grants URF/1/3437-01-01, URF/1/3771-01-01, and URF/1/4374-01-01. *(Corresponding author: Xiaohang Li.)*

The authors are with the Advanced Semiconductor Laboratory, King Abdullah University of Science and Technology, Thuwal 23955-6900, Saudi Arabia (e-mail: zhiyuan.liu@kaust.edu.sa; yi.lu@kaust.edu.sa; yue.wang@kaust.edu.sa; rongyu.lin@kaust.edu.sa; chenxin.xiong@kaust.edu.sa; xiaohang.li@kaust.edu.sa).

Digital Object Identifier 10.1109/JPHOT.2021.3139265

Besides, the unique polarization characteristics of the III-nitrides could compromise UV LED performance. On one hand, the polarization-induced quantum-confined Stark effect (QCSE) in multiple quantum wells (MQWs) brings about wavelength redshift and reduces electron-hole wavefunction overlap [8], [9]. To address this issue, researchers have utilized various approaches, including nonpolar and semi-polar orientations [10]; and introduced Si doping in quantum barriers (QBs) to screen the internal polarization induced by the electric field [11]; and polarization-matched and lattice-matched MQWs have been designed [12], [13]. Besides, Shervin *et al.* modified the piezoelectric polarization and significantly improved the LED efficiency by external bending [14].

On the other hand, the positive polarization charge could exist at the interface between the last quantum barrier (LQB) and the wider-bandgap electron blocking layer (EBL), hereafter the 'LQB/EBL polarization', because of the negative heterointerface polarization difference (ΔP) [15]. The positive charge can bend the LQB bands, resulting in a lower effective electron barrier and higher effective hole barrier. Therefore, the electron blocking and hole injection could be seriously compromised, ultimately contributing to poorer optical power and efficiency [16].

To mitigate the issue, two methods have been proposed. One is to adopt a more complex LQB or EBL structure to mitigate the LQB band bending. Qian *et al.* proposed the superlattice LQB and Zhang *et al.* designed the composition graded EBL [17], [18]. The other is to design different heterojunctions utilizing polarization engineering. For instance, lattice-matched InAlN and polarization-matched AlInGaN were used as EBLs in InGaN-based visible LEDs [19], [20]. However, the improvement by the lattice-matched InAlN EBL (i.e., without piezoelectric polarization) is limited because the positive charges still exist at the LQB/EBL interface due to the spontaneous polarization difference; and it is challenging to control the composition precisely for the polarization-matched EBL. Besides, Ji and Lin *et al.* showed that the polarization-reversed AlInGaN EBL with the negative polarization charges at the LQB/EBL interface could enhance the effective electron barrier. But it still needs to overcome the complex growth technique for the quaternary alloy [21], [22]. For UV LEDs, however, the polarization-matched or -reversed structures addressing the LQB/EBL polarization are rarely reported [23]. Besides, the N-polar and p-down design DUV LEDs were demonstrated to have better electron blocking due to the enhanced electron barrier in the EBL [24], [25].

In this work, the polarization and bandgap properties of InAlN and InAlN/AlGaN heterojunctions are first studied. The unique

This work is licensed under a Creative Commons Attribution 4.0 License. For more information, see https://creativecommons.org/licenses/by/4.0/

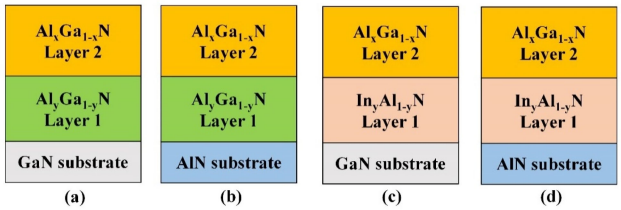

Fig. 1. The $Al_yGa_{1-y}N/Al_xGa_{1-x}N$ and $In_yAl_{1-y}N/Al_xGa_{1-x}N$ heterojunctions fully strained on GaN (a), (c) and AlN (b), (d) substrates.

relationships between the bandgap difference (ΔE_g) and the polarization difference (ΔP) of InAlN/AlGaN heterojunctions are revealed, which is hopefully applied in various devices. To further demonstrate it, the InAlN alloys are proposed as the LQBs to modulate the LQB/EBL polarization for UV LEDs. As a result, the effective electron and hole barrier are enlarged and decreased, respectively, promoting electron confinement and hole injection.

II. Polarization Engineering of InAlN/AlGaN Heterojunctions

To realize enhanced electron blocking and hole injection, the ΔE_g and the ΔP of the LQB/EBL heterojunctions need to be considered simultaneously. For instance, one could modulate the LQB/EBL polarization through changing the composition of the two layers; however, this should be conducted under the condition that the EBL bandgap is wider than the LQB (for the type I heterojunction) to block electrons effectively. Moreover, if we design polarization-matched MQWs by employing different materials as QBs, it is essential that the bandgap of QBs are larger than QWs. Consequently, the InAlN/AlGaN heterojunction is a hopeful candidate because InAlN possesses a large range of bandgap and different polarization from AlGaN. In this section, we have systematically studied the bandgap and polarization properties of the InAlN/AlGaN heterojunctions and make comparison with the conventional AlGaN/AlGaN heterojunctions.

The investigated structures are shown in Fig. 1(a)–(d). In Fig. 1(a) and (b), $Al_yGa_{1-y}N$ (layer 1) is firstly deposited on GaN or AlN substrates followed by another $Al_xGa_{1-x}N$ layer (layer 2). Both layers are fully strained on the substrates. The $In_yAl_{1-y}N/Al_xGa_{1-x}N$ heterojunctions are used for comparison in Fig. 1(c) and (d). In general, the n-type AlGaN layer of UV LEDs is thick enough (about few micrometers) such that the active region and the EBL grown on it could be partially or fully strained on the n-AlGaN layer. That means they have a similar lattice constant as that of the n-AlGaN layer, which would be used to calculate the piezoelectric polarization. Besides, the Al composition of the n-AlGaN layer varies according to the operation wavelength of the UV LED, which could be within 5% for the UVA LED, about 30% for UVB LED, and more than 50% for the UVC LED. Hence in this study, GaN and AlN substrates corresponding to the largest and smallest lattice constant in the AlGaN material system are chosen as two extreme cases to calculate the piezoelectric polarization and total polarization. It could reveal the general properties and trends of

TABLE I
The Constants Related to the Calculation of P_{SP} and P_{PZ} of $Al_XGa_{1-X}N$ and $In_YAl_{1-Y}N$ From [26]

Parameters	$Al_xGa_{1-x}N$ ($0\le x\le 1$)	$In_yAl_{1-y}N$ ($0\le y\le 1$)
a (Å)	$0.01589x^2$-0.08416x+3.182	$0.05298y^2$+0.37398y+3.109
P_{sp} (C/m^2)	$0.0072x^2$-0.0127x+1.3389	$0.1563y^2$-0.3323y+1.3402
e_{33} (C/m^2)	$0.3949x^2$+0.6324x+0.6149	$0.9329y^2$-1.5036y+1.6443
e_{31} (C/m^2)	$-0.0573x^2$-0.2536x-0.3582	$-0.0959y^2$+0.239y-0.6699
C_{13} (GPa)	112x+104(1-x)	88y+112(1-y)
C_{33} (GPa)	383x+376(1-x)	233y+383(1-y)

TABLE II
The Possible Situations of the ΔP-ΔE_G of Investigated Heterojunctions

Situation	Type	Situation	Type	Situation	Type
$\Delta P>0$ $\Delta E_g>0$	A	$\Delta P=0$ $\Delta Eg>0$	D	$\Delta P<0$ $\Delta E_g>0$	G
$\Delta P>0$ $\Delta E_g=0$	B	$\Delta P=0$ $\Delta Eg=0$	E	$\Delta P<0$ $\Delta E_g=0$	H
$\Delta P>0$ $\Delta E_g<0$	C	$\Delta P=0$ $\Delta Eg<0$	F	$\Delta P<0$ $\Delta E_g<0$	I

$In_yAl_{1-y}N/Al_xGa_{1-x}N$ heterojunctions on n-AlGaN substrates instead of focusing on one specific operation wavelength. For the specific n-AlGaN substrate, one could modify the corresponding lattice constant to calculate the polarization.

$$P_{total} = P_{sp} + P_{pz} = P_{sp} + 2\left(e_{31} - P_{sp} - \frac{c_{13}}{c_{33}}e_{33}\right)\frac{a_{sub} - a_{layer}}{a_{layer}} \ (\mathrm{C}/m^2) \quad (1)$$

$$\Delta P_{Layer2/Layer1} = P_{Layer2} - P_{Layer1} \ (\mathrm{C}/m^2) \quad (2)$$

$$b = 20.15356\exp\left(\frac{-y}{0.04012}\right) + 12.82116\exp\left(\frac{y}{0.23357}\right) + 3.64629 \quad (3)$$

$$\Delta E_{g\,Layer2/Layer1} = E_{g\,Layer2} - E_{g\,Layer1} \ (\mathrm{eV}) \quad (4)$$

The spontaneous and piezoelectric polarization (P_{sp} and P_{pz}) parameters as well as the in-plane lattice constants (a) of AlGaN and InAlN are obtained from [26] shown in Table I. The e_{31} and e_{33} are the piezoelectric constants and the C_{13} and C_{33} are the elastic constants of the epitaxial layers. The total polarization P_{total} is defined as the sum of the spontaneous and piezoelectric polarization, which could be calculated using (1). Based on the total polarization of layers 1 and 2, the ΔP is defined in (2). The positive ΔP corresponds to negative sheet interface charges and the negative ΔP corresponds to positive polarization charges. The bandgap bowing parameter (b) of the $In_yAl_{1-y}N$ alloys ($0\le y\le 1$) is extracted from the studies by Schultz *et al.* [27] shown in the (3); and the bandgaps of AlN, GaN, and InN are also from [27]. The bowing parameter of the AlGaN bandgap is from [28].The heterojunction ΔE_g is defined in (4). According to the sign of the ΔP and the ΔE_g in Eqs. (2) and (4), there are nine types of situations shown in Table II with the labels from A to I.

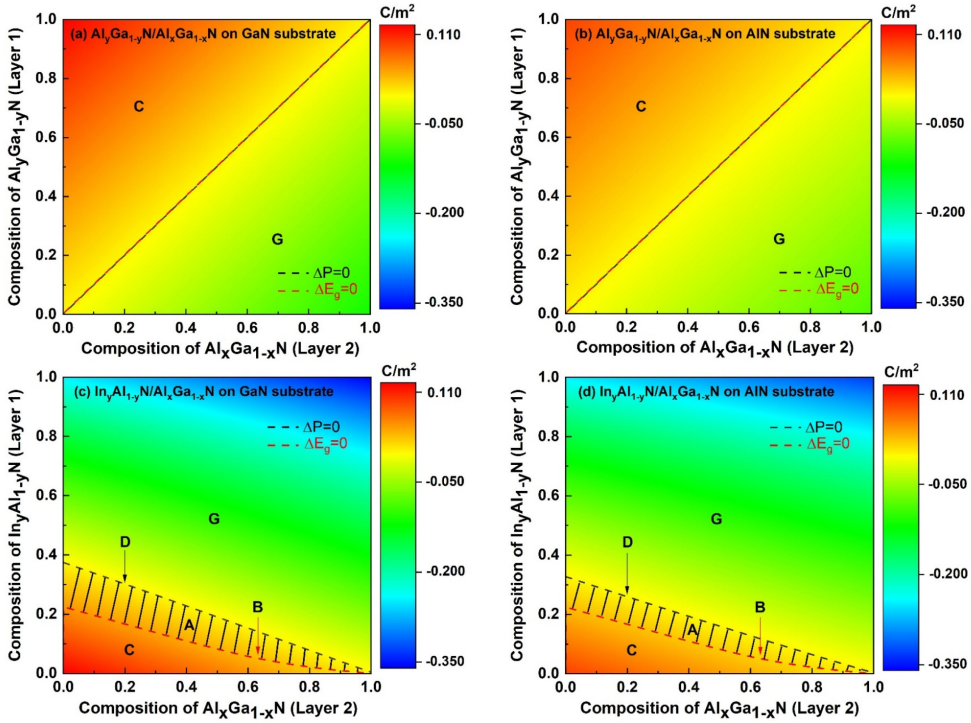

Fig. 2. The different situations of the ΔP-ΔE_g labeled from A to I of the $Al_yGa_{1-y}N/Al_xGa_{1-x}N$ and $In_yAl_{1-y}N/Al_xGa_{1-x}N$ heterojunctions fully strained on GaN (a), (c) and AlN (b), (d) substrates. The mapped region is the ΔP intensity (C/m^2). The black dash line represents $\Delta P = 0$ and the red dash line represents $\Delta E_g = 0$. For the $Al_yGa_{1-y}N/Al_xGa_{1-x}N$ heterojunctions, the dash line with $\Delta E_g = 0$ and $\Delta P = 0$ overlap each other. The shaded area is the Type A region, which is utilized to design the UVB LED in the later part.

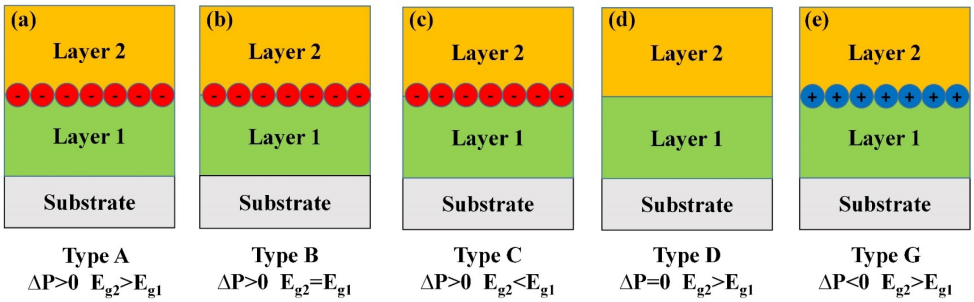

Fig. 3. Five types of situations (A, B, C, D, and G) between the ΔP and the ΔE_g (ΔP-ΔE_g) found in the investigated heterojunctions.

The ΔP-ΔE_g situation diagrams are shown in Fig. 2(a) to (d). For the $Al_yGa_{1-y}N/Al_xGa_{1-x}N$ heterojunctions in Fig. 2(a) and (b), there are only two types of situations (C and G), which are shown in Fig. 3(c) and (e) and widely found in AlGaN-based devices such as the QB on the QW and the EBL on the LQB in UV LEDs. The dash lines with $\Delta P = 0$ correspond to the $Al_yGa_{1-y}N/Al_xGa_{1-x}N$ (x = y) homojunction. For the $In_yAl_{1-y}N/Al_xGa_{1-x}N$ heterojunctions in Fig. 2(c) and (d), there are five situations in total (A, B, C, D, and G) shown in Fig. 3(a) to (e). For Types C and G, the $In_yAl_{1-y}N/Al_xGa_{1-x}N$ are similar to $Al_yGa_{1-y}N/Al_xGa_{1-x}N$.

In particular, Type D means no polarization sheet charges but with band discontinuity at the heterointerface, which is on the dash line with $\Delta P = 0$ in the situation diagram. It could be used to design polarization-matched structures such as MQWs to eliminate the QCSE. The two layers of Type B have the same bandgap, but with polarization sheet charges at the heterointerface, which is expected to be used in some specially designed structures. For Type A (shaded region in Fig. 2), the $Al_xGa_{1-x}N$ layer has a wider bandgap compared with the $In_yAl_{1-y}N$ layer and the sheet charges at the heterointerface are negative, which is the polarization-reversed structure mentioned above and could be applied to the LQB/EBL heterojunction. In this study, we utilize this unique property to design InAlN LQBs to replace the conventional AlGaN LQB to modulate the LQB/EBL polarization in the 320 nm UVB LED as a special case. Additionally, it is observed that the Type A situation covers all Al content of the AlGaN layer. Thus, this method could be easily extended to LEDs and LDs in other UV regions.

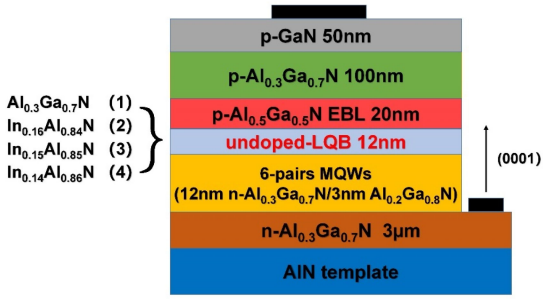

Fig. 4. The cross-sectional schematic structure of UV LEDs with various LQBs.

III. LED Structure and Parameters

The cross-sectional schematic structure of the 320 nm UVB LEDs, including the conventional AlGaN LQB and proposed InAlN LQBs used in the simulation are shown in Fig. 4. For the conventional structure (Device 1), a 3 μm n-type $Al_{0.3}Ga_{0.7}N$ layer doped with Si of $5\times10^{18}/cm^3$ is grown on the AlN template. It is followed by six pairs of AlGaN/AlGaN MQWs comprising 12 nm $Al_{0.3}Ga_{0.7}N$ QBs and 3 nm $Al_{0.2}Ga_{0.8}N$ QWs. $5\times10^{17}/cm^3$ silicon doping in QBs except the LQB is included to screen the QCSE [29]. The LQB is not doped in that it could reduce the effective electron barrier and increase the electron leakage [30]. Above the LQB is the 20 nm p-type $Al_{0.5}Ga_{0.5}N$ layer EBL and the 100 nm p-type $Al_{0.3}Ga_{0.7}N$ hole injection layer. The Mg doping concentrations are $5\times10^{18}/cm^3$ and $3\times10^{19}/cm^3$, respectively. Finally, a 50 nm p-type GaN contact layer with the Mg doping concentration of $1\times10^{20}/cm^3$ caps the structure. The mesa size of the devices in the simulation is 300 μm $\times$ 300 μm. For the proposed structures, they are the same as Device 1 except for the use of $In_{0.16}Al_{0.84}N$ (Device 2), $In_{0.15}Al_{0.85}N$ (Device 3), and $In_{0.14}Al_{0.86}N$ (Device 4) as the LQB to examine and modulate the LQB/EBL ΔP for various electron blocking and hole injection capabilities.

The APSYS software by Crosslight is employed in this study to self-consistently solve various physical equations including drift-diffusion equations, Schrodinger and Poisson's equations, current continuity equations, etc. with proper boundary conditions [31].

The AlGaN band offset ratio is set to be 0.65/0.35 [32]. The electron affinity of the InAlN alloys is from [27]. The Shockley-Read-Hall (SRH) recombination lifetime and the Auger recombination coefficient are 50 ns and $1.0\times10^{-30}/cm^3$ [33]. A 0.6 polarization screening factor is set because the interface charge density obtained from the experiment is usually smaller than the theoretical value due to the screening of defects and injected carriers [34], [35]. The operating temperature and background loss are separately estimated to be 300 K [36] and 2000 m^{-1} [37]. The activation energy of GaN and AlGaN are set to be 170 and 270 meV [38], [39]. Besides, we assume that the 3 μm n-$Al_{0.3}Ga_{0.7}N$ layer is fully relaxed on the AlN template and other layers are fully strained on the n-layer. The LQB/EBL ΔP without the effect of the polarization screening factor and the bandgaps of Devices 1 to 4 are shown in Table III. Although from the calculation, the ΔP between $In_{0.18}Al_{0.82}N$ and $Al_{0.5}Ga_{0.5}N$ is the smallest (0.0003 C/m^2), we do not use $In_{0.18}Al_{0.82}N$ as LQB in this study because its bandgap is smaller than the $Al_{0.2}Ga_{0.8}N$ quantum well (3.830 eV) and could not confine carriers as the QB. Other parameters used in this work are based on the default values in APSYS.

TABLE III
The LQB/EBL ΔP Without the Effect of the Polarization Screening Factor and LQB Bandgaps of Different Devices

Device ID	LQB	LQB/EBL ΔP (C/m^2)	Bandgap (eV)
1	$Al_{0.3}Ga_{0.7}N$	-0.0207	4.058
2	$In_{0.16}Al_{0.84}N$	0.0061	3.882
3	$In_{0.15}Al_{0.85}N$	0.0090	3.980
4	$In_{0.14}Al_{0.86}N$	0.0119	4.041

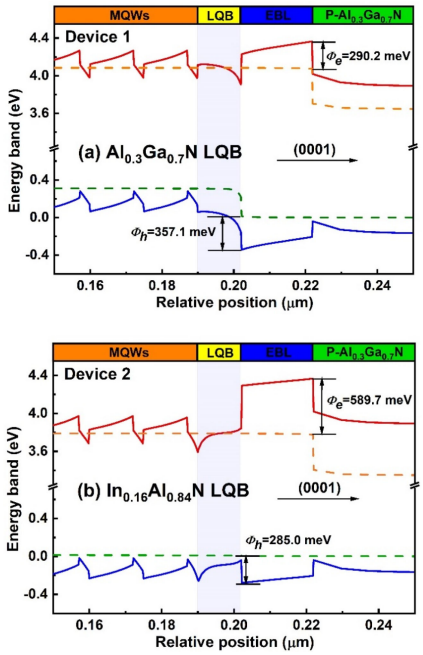

Fig. 5. Calculated band edge profiles at 60 mA (67 A/cm^2) of (a) Device 1 with the $Al_{0.3}Ga_{0.7}N$ LQB and (b) Device 2 with the $In_{0.16}Al_{0.84}N$ LQB. The shaded area is the LQB.

IV. Result and Discussion

The band diagrams of Devices 1 and 2 are plotted in Fig. 5(a) and (b). Fig. 5(a) shows that due to the negative LQB/EBL ΔP (-0.0207 C/m^2), the positive sheet charges accumulate at the heterointerface. The conduction and valence bands of the LQB near the EBL of Device 1 bend down and up significantly, resulting in 290.2 and 357.1 meV effective barrier heights for electrons and holes, respectively. The limited effective electron barrier indicates that electrons could move over the barrier leading to considerable electron overflow; and the large effective hole barrier could pose major challenges for holes to inject into the active region. For Device 2 in Fig. 5(b), the $In_{0.16}Al_{0.84}N/Al_{0.5}Ga_{0.5}N$ ΔP is positive and lower (0.0061 C/m^2) compared with Device 1 and only a small amount of negative polarization charges localize at the heterointerface. Thus, the band bending direction

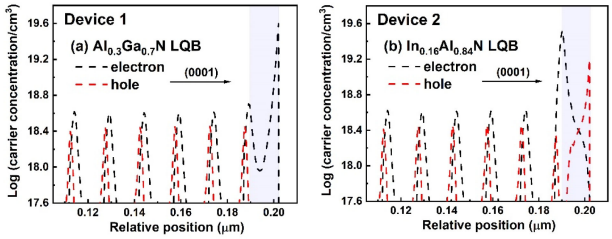

Fig. 6. Log scale electron and hole concentrations in MQWs at 60 mA (67 A/cm^2) of (a) Device 1 with the $Al_{0.3}Ga_{0.7}N$ LQB and (b) Device 2 with the $In_{0.16}Al_{0.84}N$ LQB. The shaded area is the LQB.

in the LQB is opposite to that of Device 1 and the bands near the EBL are much flatter. It brings about a higher barrier for electrons and a lower barrier for holes, about 589.7 and 285.0 meV, respectively.

To reveal the electron and hole distribution of Device 1 and Device 2, we calculate the carrier concentration across the active region shown in Fig. 6(a) and (b). It indicates that an electron peak is observed in the LQB of Device 1, which is consistent with the electrostatic field profile and band bending effects at the LQB/EBL interface. For Device 2, it is observed that a hole peak exists in the LQB due to the downward bending; and the electron concentration in the last quantum well (LQW) is quite high because of the downward bending of the conduction band as a result of the larger LQW/LQB ΔP. Although Device 2 has the higher barrier for electrons and the lower barrier for holes thanks to the polarization modulation, the carrier concentration in the first five QWs is similar with Device 1 because of the accumulation of electrons and holes in the LQW and the LQB, respectively. As mentioned above, the bands are flat enough in the LQB of Device 2 thus the energy variety is diminutive. Therefore, the high-level electron concentration in the LQW could be extended to the LQB to a certain extent. Similar concentration extension could be also observed for holes. The overlapping of electrons and holes could generate the extra recombination in the LQB and could be proven by the radiative recombination distribution shown later.

The situations are different for Devices 3 and 4 as Fig. 7 and Fig. 8 show. It is observed there are still an electron and a hole peak in the LQW and the LQB respectively. But owing to the bigger positive LQB/EBL ΔP (0.0090 and 0.0119 C/m^2) as well as the larger LQW/LQB ΔP compared with Device 2, the conduction and valence band in the LQB sharply bends upward and downward, respectively, causing the quicker energy change in the LQB and less carrier concentration between the electron and hole concentration peaks. Therefore, there would be less or no recombination in the $In_{0.15}Al_{0.85}N$ and $In_{0.14}Al_{0.86}N$ LQBs. The carrier concentration in MQWs of Devices 3 and 4 also improves. The electron barrier heights for Device 3 (568.7 meV) and Device 4 (547.0 meV) are lower than that of Device 2 (575 meV), but the hole barrier (244.4 and 214.0 meV) in EBL is lower. Besides, as shown in Fig. 7 and Table IV, although there are higher hole barriers in $In_{0.15}Al_{0.85}N$ and $In_{0.14}Al_{0.86}N$ LQB (337.3 and 416.0 meV), the blocking for holes is limited because

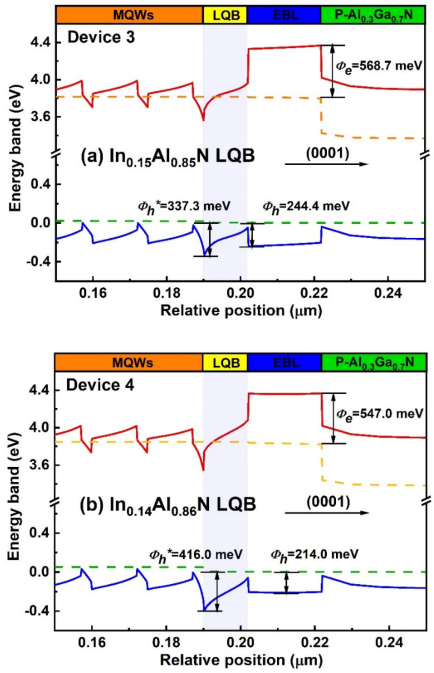

Fig. 7. Calculated band edge profiles at 60 mA (67 A/cm^2) of (a) Device 3 with the $In_{0.15}Al_{0.85}N$ LQB and (b) Device 4 with the $In_{0.14}Al_{0.86}N$ LQB. The shaded area is the LQB.

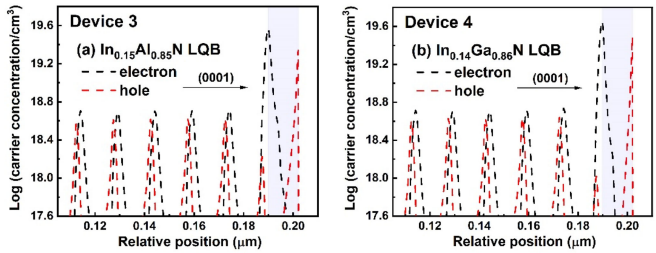

Fig. 8. Log scale electron and hole concentrations in MQWs at 60 mA (67 A/cm^2) of (a) Device 3 with the $In_{0.15}Al_{0.85}N$ LQB and (b) Device 4 with the $In_{0.14}Al_{0.86}N$ LQB. The shaded area is the LQB.

TABLE IV
THE EFFECTIVE ELECTRON BARRIER Φ_E AND EFFECTIVE HOLE BARRIER Φ_H IN DIFFERENT DEVICES

Device ID	Φ_e in EBL (meV)	Φ_h in EBL (meV)	Φ_h in LQB (meV)
1	290.2	357.1	/
2	589.7	285.0	/
3	568.7	244.4	337.3
4	547.0	214.0	416.0

the width of the LQB is narrower than the EBL. And numerically, they are still competitive compared with the hole barrier height in Device 1.

The radiative recombination rate in the fifth QW, sixth QW (LQW), and LQB of Devices 1 to 4 are shown in Fig. 9(a). The radiative recombination rate in the previous four QWs are similar with the fifth one thus not shown in the figure. In the first five QWs, Device 1 has the lowest radiative recombination rates and the average is about 1.9×10^{26} cm^{-3}/s. Inversely, the average

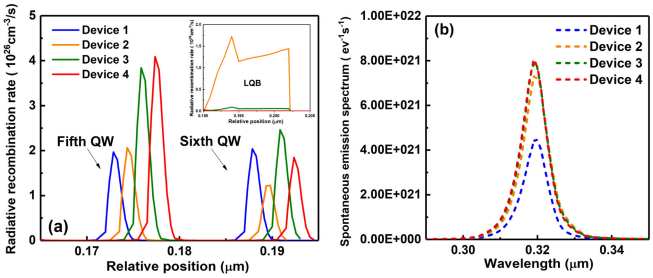

Fig. 9. (a) Radiative recombination rate and (b) Spontaneous emission rates of AlGaN and InAlN LQB structures at 60 mA (67 A/cm^2). For radiative recombination rate in the fifth and sixth QW, the horizontal positions of Devices B, C, and D have been shifted slightly for better observation.

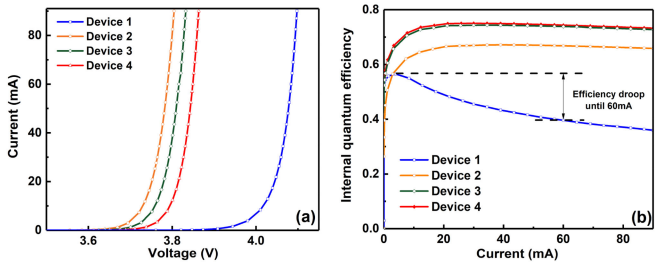

Fig. 10. (a) I-V characterization curve and (b) internal quantum efficiency of conventional and proposed LEDs.

TABLE V
THE INTERNAL QUANTUM EFFICIENCY, EFFICIENCY DROOP, OPTICAL OUTPUT POWER, AND WALL PLUG EFFICIENCY OF DIFFERENT DEVICES AT 60 MA (67 A/CM^2)

	Device 1	Device 2	Device 3	Device 4
Peak IQE	56.6%	67.2%	74.4%	75.0%
IQE droop	16.9%	0.3%	0.5%	0.7%
Output power (mW)	92.5	161.1	172.4	173.7
WPE	3.78%	7.09%	7.53%	7.52%

rate of Device 4 is the highest (3.9×10^{26} cm^{-3}/s) because of more carriers in MQWs, which are over two times than those of Device 1. As for Devices 2 and 3, the high-level carrier concentration in the LQW and the LQB only produce little recombination because the distance between the peaks of electron and hole is about 12 nm (the QB width) and only a part of carriers between the two peaks can generate recombination effectively. It also causes a worse average radiative recombination rate in the first five QWs (2.0×10^{26} and 3.7×10^{26} cm^{-3}/s) compared to Device 4. Thus, although the radiative recombination in the LQB of Device 2 is a part of improvement origin relative to Device 1, Devices 3 and 4 distribute more carriers to MQWs instead of accumulating in the LQB. And this improves the overall radiative recombination intensity and efficiency compared with Device 2. It is noted that the recombination rates in the LQW of the proposed structures are suppressed due to the low hole concentration. However, the overall performance of the proposed structures is better compared with the conventional one, which could be proven by the total spontaneous emission rate shown in Fig. 9(b). Besides, no obvious wavelength shift is observed in the proposed devices. These results are consistent with our analysis on the band diagram and carrier concentration above. We believe that $In_{0.15}Al_{0.85}N$ and $In_{0.14}Al_{0.86}N$ LQB LEDs could have better performance due to the better electron blocking and hole injection and less carrier accumulation and recombination in the LQB.

Fig. 10 (a) shows the I-V characteristic of four different structures. It indicates that better electron confinement and hole injection contribute to lower operation voltage at the same current in proposed structures, which means lower power consumption in LED. It is worth noting that in comparison with Device 2, the operation voltage is larger in Devices 3 and 4 because of the lower effective electron barrier in EBLs and higher hole injection barrier in LQBs.

At last, we calculate the internal quantum efficiency (IQE), efficiency droop, optical output power, and wall plug efficiency (WPE) of Devices 1-4 shown in Fig. 10(b) and Table V, respectively.

The proposed structures have a higher IQE and less efficiency droop compared with the conventional one. Device 4 shows the best performance among all the structures owing to better carrier transportation and more effective recombination in MQWs. Its peak IQE reaches about 75.0% and the efficiency droop is within 1% until 60 mA. The output power also shows the same trend. It is worth noting that Device 3 and Device 4 have slightly higher efficiency droop compared with Device 2. Similar to the operation voltage, this is also due to the lower effective electron barrier in the EBL and the higher hole injection barrier in the LQB in Devices 3 and 4, which could influence on the injection efficiency at the high injection current. The WPE of Device 3 is a little bit higher than Device 4 in our calculation due to the lower operation voltage. For other InAlN LQBs with lower indium composition such as $In_{0.13}Al_{0.87}N$ and $In_{0.12}Al_{0.88}N$, it does little to further reduce the accumulation and recombination of carriers in the LQB. And it will contribute to more serious blocking for holes because of a higher hole barrier in the LQB induced by the larger LQW/LQB ΔP, ultimately leading to the higher operation voltage, more serious IQE droop, and the poorer WPE. Thus, we conclude that all proposed structures have much better performance compared with the conventional structure and InAlN LQBs with 0.14 and 0.15 indium composition are more suitable to replace the conventional AlGaN LQB in the 320 nm UVB LED. As mentioned above, for more general cases, InAlN with other In contents could be chosen to modulate the polarization and achieve high efficiency UV LEDs in other UV regions.

Previously, the InAlN alloys have been regarded as a promising material for LEDs at different wavelengths. It has been demonstrated that $In_{0.18}Al_{0.82}N$ is nearly lattice-matched with GaN and could bring about a better performance when used as the EBL in visible LEDs [40]. Moreover, the InAlN alloys could be applied to UV LEDs with lower indium compositions and thus larger bandgap [41]. On the other hand, it is not straightforward to grow high quality InAlN because of phase separation and composition inhomogeneity [42], [43]. Nevertheless, high quality InAlN LEDs and power devices with lower indium compositions have been achieved. Anna *et al.* reported

the $In_{0.14}Al_{0.86}N$ /AlN/GaN high electron mobility transistor (HEMT) [44] and Pietro *et al.* fabricated the UVA LED with $In_{0.14}Al_{0.86}N$ polarization matched quantum well [45]. Thus, we believe our design could effectively improve the polarization issue in AlGaN-based UV LED without introducing complex structures and growth techniques.

V. Conclusion

Polarization modulation and band engineering are powerful methods for achieving high efficiency III-nitride devices. In this work, the different situations of the InAlN/AlGaN heterojunction ΔP-ΔE_g fully strained on AlN and GaN substrates are investigated. The InAlN/AlGaN heterojunctions exhibit three unique ΔP-ΔE_g situations: $\Delta P>0$, $\Delta E_g>0$ (A); $\Delta P>0$, $\Delta E_g = 0$ (B); and $\Delta P = 0$, $\Delta E_g>0$ (D), which could not be realized by the common AlGaN/AlGaN heterojunctions. This special property is expected to apply to the design of distinctive devices such as LED and LD. As a specific example of Type A, the InAlN last quantum barrier with 0.14–0.16 indium composition substituting for the conventional AlGaN LQB in the 320 nm UVB LED have been numerically studied. The simulation results indicate that by the polarization modulation, the effective electron barrier is enlarged drastically from 290.2 to more than 547.0 meV and the effective hole barrier is also significantly decreased. Thus, the proposed structures have better optical performance attributed to the improvement of electron confinement and hole injection. By properly decreasing indium composition from 0.16, much higher IQE and WPE could be achieved. The method could be extended to other UV regions through appropriately choosing the composition of the InAlN LQB and AlGaN EBL based on the ΔP-ΔE_g diagram. This theoretical work provides a new horizon and perspective for development of high efficiency UV LEDs.

References

[1] M. Kneissl and J. Rass, "A brief review of III-Nitride UV emitter technologies and their applications," in *III-Nitride Ultraviolet Emitters: Technology and Applications*, Berlin, Germany: Springer, 2016, pp. 1–4.

[2] F. Nippert *et al.*, "Auger recombination in AlGaN quantum wells for UV light-emitting diodes," *Appl. Phys. Lett.*, vol. 113, no. 7, Aug. 2018, Art. no. 071107.

[3] K. Ban *et al.*, "Internal quantum efficiency of whole-composition-range AlGaN multiquantum wells," *Appl. Phys. Exp.*, vol. 4, no. 5, Apr. 2011, Art. no. 052101.

[4] Y. K. Kuo, J. Y. Chang, F. M. Chen, Y. H. Shih, and H. T. Chang, "Numerical investigation on the carrier transport characteristics of AlGaN deep-UV light-emitting diodes," *IEEE J. Quantum Electron*, vol. 52, no. 4, Feb. 2016, Art. no. 3300105.

[5] M. Kneissl and J. Rass, "Impacts of dislocations and point defects on the internal quantum efficiency of the near-band-edge emission in AlGaN-Based DUV Light-emitting materials," in *III-Nitride Ultraviolet Emitters: Technology and Applications*. Berlin, Germany: Springer, 2016, pp. 115–136.

[6] Z. Ren *et al.*, "III-nitride deep UV LED without electron blocking layer," *IEEE Photon. J.*, vol. 11, no. 2, Mar. 2019, Art. no. 8200511.

[7] Q. Chen *et al.*, "Enhanced optical performance of AlGaN-based deep ultraviolet light-emitting diodes by electrode patterns design," *IEEE Electron Device Lett.,* vol. 40, no. 12, pp. 1925–1928, Oct. 2019.

[8] M. F. Schubert *et al.*, "Polarization-matched GaInN/AlGaInN multi-quantum-well light-emitting diodes with reduced efficiency droop," *Appl. Phys. Lett.*, vol. 93, no. 4, Jul. 2008, Art. no. 041102.

[9] F. Wu *et al.*, "Significant internal quantum efficiency enhancement of GaN/AlGaN multiple quantum wells emitting at ∼350 nm via step quantum well structure design," *J. Phys. D—Appl. Phys.*, vol. 50, no. 24, May 2017, Art. no. 245101.

[10] J. Bruckbauer *et al.*, "Spatially-resolved optical and structural properties of semi-polar $al_xGa_{1-x}N$ with x up to 0.56," *Sci. Rep.*, vol. 7, Sep. 2017, Art. no. 10804.

[11] Z. H. Zhang *et al.*, "On the effect of step-doped quantum barriers in InGaN/GaN light emitting diodes," *J. Disp. Technol.*, vol. 9, no. 4, pp. 226–233, Jul. 2012.

[12] H. H. Yao *et al.*, "Polarization matched c-plane III-nitride quantum well structure," in *Proc. SPIE*, San Francisco, CA, USA, 2019, Art. no. 109400K.

[13] N. Wang, Y. A. Yin, B. Zhao, and T. Mei, "Performance analysis of GaN-based light-emitting diodes with lattice-matched InGaN/AlInN/InGaN quantum-well barriers," *J. Disp. Technol.*, vol. 11, no. 12, pp. 1056–1060, Jun. 2015.

[14] S. Shervin *et al.*, "Flexible deep-ultraviolet light-emitting diodes for significant improvement of quantum efficiencies by external bending," *J. Phys. D—Appl. Phys.*, vol. 51, no. 10, Feb. 2018, Art. no. 105105.

[15] C. Chu *et al.*, "On the origin of enhanced hole injection for AlGaN-based deep ultraviolet light-emitting diodes with AlN insertion layer in p-electron blocking layer," *Opt. Exp.*, vol. 27, no. 12, pp. A620–A628, Jun. 2019.

[16] L. Y. Wang *et al.*, "Efficiency enhancement of ultraviolet light-emitting diodes with segmentally graded p-type AlGaN layer," *Chin. Phys. B*, vol. 28, no. 1, Jan. 2019, Art. no. 018503.

[17] Q. Chen *et al.*, "Improved the AlGaN-based ultraviolet LEDs performance with super-lattice structure last barrier," *IEEE Photon. J.*, vol. 10, no. 4, Jul. 2018, Art. no. 8201007.

[18] Z. H. Zhang *et al.*, "Increasing the hole energy by grading the alloy composition of the p-type electron blocking layer for very high-performance deep ultraviolet light-emitting diodes," *Photon. Res.*, vol. 7, no. 4, pp. B1–B6, Apr. 2019.

[19] H. J. Kim *et al.*, "Improvement of quantum efficiency by employing active-layer-friendly lattice-matched InAlN electron blocking layer in green light-emitting diodes," *Appl. Phys. Lett.*, vol. 96, no. 10, Mar. 2010, Art. no. 101102.

[20] Y. K. Kuo, M. C. Tsai, and S. H. Yen, "Numerical simulation of blue InGaN light-emitting diodes with polarization-matched AlGaInN electron-blocking layer and barrier layer," *Opt. Commun.*, vol. 282, no. 21, pp. 4252–4255, Nov. 2009.

[21] Z. Lin *et al.*, "Achieving high-performance blue GaN-based light-emitting diodes by energy band modification on $al_xIn_yGa_{1-x-y}N$ electron blocking layer," *IEEE Trans. Electron Devices*, vol. 64, no. 2, ppp. 472–480, Dec. 2016.

[22] X. Ji *et al.*, "Efficiency improvement by polarization-reversed electron blocking structure in GaN-based light-emitting diodes," *Opt. Exp.*, vol. 22, no. S3, pp. A1001–A1008, May 2014.

[23] X. Ji *et al.*, "Tailoring of energy band in electron-blocking structure enhancing the efficiency of AlGaN-based deep ultraviolet light-emitting diodes," *IEEE Photon. J.*, vol. 8, no. 3, Apr. 2016, Art. no. 1600607.

[24] H. Tao, S. Xu, X. Fan, J. Zhang, and Y. Hao, "Greatly enhanced wall-plug efficiency of N-polar AlGaN-based deep ultraviolet light-emitting diodes," *IEEE Photon. J.*, vol. 13, no. 3, Jun. 2021, Art. no. 8200311.

[25] Y. Lu, C. Wang, V. P. De Oliveira, Z. Liu, and X. Li, "UV light-emitting diode with buried polarization-induced n-AlGaN/InGaN/p-AlGaN tunneling junction," *IEEE Photon. Technol. Lett.*, vol. 33, no. 16, pp. 808–811, Aug. 2021.

[26] K. Liu and X. Li, "Polarization properties of wurtzite III nitride indicates the principle of polarization engineering," Jan. 2020, *arXiv:1808.07211v4*.

[27] S. Schulz *et al.*, "Composition-dependent band gap and band-edge bowing in alinn: A combined theoretical and experimental study," *Appl. Phys. Exp.*, vol. 6, no. 12, Nov. 2013, Art. no. 121001.

[28] C. Coughlan, S. Schulz, M. A. Caro, and E. P. O'Reilly, "Band gap bowing and optical polarization switching in AlGaN alloys," *Phys. Status Solidi B*, vol. 252, no. 5, pp. 879–884, May 2015.

[29] K. Tian *et al.*, "Investigations on AlGaN-based deep-ultraviolet light-emitting diodes with si doped quantum barriers of different doping concentrations," *Phys. Status Solidi Rapid Res. Lett.*, vol. 12, no. 1, Jan. 2018, Art. no. 1700346.

[30] L. Lu *et al.*, "Performance improvement of AlGaN-based deep-ultraviolet light-emitting diodes via Si-doping design of quantum barriers," *Superlattices Microstruct,* vol. 109, pp. 687–692, Sep. 2017.

[31] APSYS, Crosslight Software, Burnaby, BC, Canada, 2017. Accessed: Oct. 2019. [Online]. Available: http://www.crosslight.com

[32] D. R. Hang *et al.*, "$Al_xGa_{1-x}N$/GaN band offsets determined by deep-level emission," *J. Appl. Phys.*, vol. 90, no. 4, pp. 1887–1890, Aug. 2001.
[33] J. Piprek, F. Römer, and B. Witzigmann, "On the uncertainty of the auger recombination coefficient extracted from InGaN/GaN light-emitting diode efficiency droop measurements," *Appl. Phys. Lett.*, vol. 106, no. 10, Mar. 2015, Art. no. 101101.
[34] S. Wang *et al.*, "Graded AlGaN/AlGaN superlattice insert layer improved performance of AlGaN-based deep ultraviolet light-emitting diodes," *J. Disp. Technol.*, vol. 12, no. 10, pp. 1112–1116, Jun. 2016.
[35] J. Piprek, T. M. Katona, S. P. DenBaars, and S. Li, "3D simulation and analysis of AlGaN/GaN ultraviolet light-emitting diodes," in *Proc. SPIE*, San Jose, CA, USA, 2004, pp. 127–136.
[36] T. Lu *et al.*, "Effect of the thickness of undoped GaN interlayers between multiple quantum wells and the p-doped layer on the performance of GaN light-emitting diodes," *Opt. Exp.*, vol. 19, no. 19, pp. 18319–18323, Sep. 2011.
[37] V. Fiorentini, F. Bernardini, and O. Ambacher, "Evidence for nonlinear macroscopic polarization in III–V nitride alloy heterostructures," *Appl. Phys. Lett.*, vol. 80, no. 7, pp. 1204–1206, Feb. 2002.
[38] W. Götz *et al.*, "Activation of acceptors in Mg-doped GaN grown by metalorganic chemical vapor deposition," *Appl. Phys. Lett.*, vol. 68, no. 5, pp. 667–669, Jan. 1996.
[39] K. B. Nam, M. L. Nakarmi, J. Li, J. Y. Lin, and H. X. Jiang, "Mg acceptor level in AlN probed by deep ultraviolet photoluminescence," *Appl. Phys. Lett.*, vol. 83, no. 5, pp. 878–880, Aug. 2003.
[40] S. Choi *et al.*, "Improvement of peak quantum efficiency and efficiency droop in III-nitride visible light-emitting diodes with an InAlN electron-blocking layer," *Appl. Phys. Lett.*, vol. 96, no. 22, May 2010, Art. no. 221105.
[41] L. Li *et al.*, "Ultrathin inserted AlGaN/InAlN heterojunction for performance improvement in AlGaN-based deep ultraviolet light-emitting diodes," *Appl. Phys. Exp.*, vol. 12, no. 1, Jan. 2019, Art. no. 011010.
[42] A. Redondo-Cubero *et al.*, "Depth-resolved analysis of spontaneous phase separation in the growth of lattice-matched AlInN," *J. Phys. D—Appl. Phys.*, vol. 43, no. 5, Jan. 2010, Art. no. 055406.
[43] H. P. D. Schenk *et al.*, "Indium incorporation dynamics into AlInN ternary alloys for laser structures lattice matched to GaN," *Appl. Phys. Lett.*, vol. 93, no. 8, Aug. 2008, Art. no. 081116.
[44] A. Malmros *et al.*, "Enhanced mobility in InAlN/AlN/GaN HEMTs using a GaN interlayer," *IEEE Trans. Electron Devices*, vol. 66, no. 7, pp. 2910–2915, Jun. 2019.
[45] P. Pampili *et al.*, "InAIN-based LEDs emitting in the near-UV region," *J. Appl. Phys.*, vol. 58, May 2019, Art. no. SCCB33.